



Blockage of the adenosine A_{2B} receptor prevents cardiac fibroblasts overgrowth in rats with pulmonary arterial hypertension

Mafalda Bessa-Gonçalves¹ · Bruno Bragança^{1,2} · Eduardo Martins-Dias¹ · Adriana Vinhas¹ · Mariana Certal¹ · Tânia Rodrigues¹ · Fátima Ferreirinha¹ · Maria Adelina Costa^{1,3} · Paulo Correia-de-Sá¹ · Ana Patrícia Fontes-Sousa¹

Received: 16 March 2023 / Accepted: 12 June 2023 / Published online: 5 July 2023
© The Author(s) 2023

Abstract

Sustained pressure overload and fibrosis of the right ventricle (RV) are the leading causes of mortality in pulmonary arterial hypertension (PAH). Although the role of adenosine in PAH has been attributed to the control of pulmonary vascular tone, cardiac reserve, and inflammatory processes, the involvement of the nucleoside in RV remodelling remains poorly understood. Conflicting results exist on targeting the low-affinity adenosine A_{2B} receptor (A_{2B}AR) for the treatment of PAH mostly because it displays dual roles in acute vs. chronic lung diseases. Herein, we investigated the role of the A_{2B}AR in the viability/proliferation and collagen production by cardiac fibroblasts (CFs) isolated from RVs of rats with monocrotaline (MCT)-induced PAH. CFs from MCT-treated rats display higher cell viability/proliferation capacity and overexpress A_{2B}AR compared to the cells from healthy littermates. The enzymatically stable adenosine analogue, 5'-N-ethylcarboxamidoadenosine (NECA, 1–30 μM), concentration-dependently increased growth, and type I collagen production by CFs originated from control and PAH rats, but its effects were more prominent in cells from rats with PAH. Blockage of the A_{2B}AR with PSB603 (100 nM), but not of the A_{2A}AR with SCH442416 (100 nM), attenuated the proliferative effect of NECA in CFs from PAH rats. The A_{2A}AR agonist, CGS21680 (3 and 10 nM), was virtually devoid of effect. Overall, data suggest that adenosine signalling via A_{2B}AR may contribute to RV overgrowth secondary to PAH. Therefore, blockage of the A_{2A}AR may be a valuable therapeutic alternative to mitigate cardiac remodelling and prevent right heart failure in PAH patients.

Keywords Pulmonary arterial hypertension · Right ventricular remodelling · Monocrotaline rat model · Adenosine A_{2B} receptor · Cardiac fibroblasts · Viability/proliferation · Collagen production

Mafalda Bessa-Gonçalves graduated in Genetics and Biotechnology (2013) and defended her MSc thesis in Technologic, Comparative and Molecular Genetics in 2015 on purinergic signalling mechanisms underlying cardiac fibrosis secondary to pulmonary arterial hypertension. She defended a PhD Thesis in Molecular and Cellular Biotechnology Applied to Health Sciences in 2022. Her PhD work was developed at i3S/INEB/UP and focused on Bioengineering an Immunomodulatory Microenvironment for Bone Healing, combining Fibrinogen and Magnesium. Nowadays, her research interests focus on advanced tissue/cellular models, immune cell therapy, cell-based assays and imaging.



This paper is dedicated to the enthusiasm, joy, and commitment of Maria Teresa Miras Portugal to the purinergic field.

Mafalda Bessa-Gonçalves and Bruno Bragança contributed equally to this manuscript.

✉ Paulo Correia-de-Sá
farmacol@icbas.up.pt

✉ Ana Patrícia Fontes-Sousa
apsousa@icbas.up.pt

- ¹ Laboratório de Farmacologia e Neurobiologia, Departamento de Imuno-Fisiologia e Farmacologia/Centro de Investigação Farmacológica e Inovação Medicamentosa (MedInUP), Instituto de Ciências Biomédicas Abel Salazar, Universidade do Porto (ICBAS-UP), R. Jorge Viterbo Ferreira, 228, 4050-313 Porto, Portugal
- ² Departamento de Cardiologia, Centro Hospitalar Tâmega e Sousa, Penafiel, Portugal
- ³ Departamento de Química, ICBAS-UP, Porto, Portugal

Abbreviations

A	Absorbance
A _{2A} AR	Adenosine A _{2A} receptor
A _{2B} AR	Adenosine A _{2B} receptor
BSA	Bovine serum albumin
CGS21680	4-[2-[[6-Amino-9-(nethyl-β-D-ribofuranuronamidoyl)-9H-purin-2-yl]amino]ethyl] benzene-propanoic acid hydrochloride
CTRL	Control
DAPI	4'-6-Diamidino-2-phenylindole
DMSO	Dimethyl sulfoxide
ECM	Extracellular matrix
FBS	Fetal bovine sérum
MCT	Monocrotaline
MTT	3-[4,5-Dimethylthiazol-2-yl]-2,5-diphenyltetrazolium bromide
NECA	5'-N-ethylcarboxamidoadenosine
PAH	Pulmonary arterial hypertension
PBS	Phosphate-buffered saline
PFA	Paraformaldehyde
PSB603	8-[4-[4-(4-Chlorophenyl)piperazine-1-sulfonyl]phenyl]-1-propylxanthine
RV	Right ventricle
SCH442416	2-(2-Furanyl)-7-[3-(4-methoxyphenyl)propyl]-7H-pyrazolo[4,3-e][1,2,4]triazolo[1,5-c]pyrimidin-5-amine

Introduction

Pulmonary arterial hypertension (PAH) is a severe cardiopulmonary disorder characterized by pulmonary vascular remodelling resulting in a progressive increase in pulmonary vascular resistance and, subsequent, increases in the right ventricle (RV) afterload [1]. If left untreated, PAH rapidly progresses, leading to RV failure and death. Although the initial impact of PAH primarily affects the pulmonary vasculature, the survival of patients with PAH is closely related to the maintenance of the RV function [1]. Despite current medical advancements, PAH still carries a poor prognosis, thus prompting the urgent need for novel molecular targets to prevent and/or control disease progression and, thereby, reduce mortality [2].

Currently approved medications for PAH primarily focus on the reduction of pulmonary vascular resistance [2, 3], but none of the available therapies directly targets RV remodelling underlying heart failure [3, 4]. Few successful attempts using miRNA-based therapies have been attempted, but these novel biotechnological approaches are far from being clinically approved for use in PAH patients [5, 6]. The RV pressure overload secondary to PAH causes adverse ventricular remodelling as a consequence of cardiac fibrosis associated with excessive

deposition of extracellular matrix (ECM) proteins [7]. Albeit interstitial cardiac fibroblasts (CFs) are the main protagonists in cardiac fibrosis, their enrolment in PAH-induced RV dysfunction remains poorly investigated, thus opening new research opportunities to address this unmet medical condition.

The purine nucleoside adenosine is a ubiquitous regulatory molecule existing both inside and outside all living cells. Adenosine controls cell functions by acting via a family of four membrane-bound G protein-coupled receptors, A₁AR, A_{2A}AR, A_{2B}AR, and A₃AR [8]. Increasing evidence suggests that the low-affinity A_{2B}AR-mediated cell signalling is deleterious for the progression of heart dysfunction secondary to lung diseases since this receptor blockade has protective effects (for a review, see, e.g., [9, 10]). In animal models of pulmonary hypertension, overexpression of the A_{2B}AR has been associated with increased levels of remodelling agents (e.g., IL-6 and matrix metalloproteinases) and signalling molecules implicated in the pathogenesis of PAH, such as endothelin-1 [11].

Data in the literature suggests that adenosine regulates myocardial remodelling by interfering with CFs proliferation and differentiation [12–14]. Indeed, CFs are endowed with all adenosine receptor subtypes [15], with high amounts of A_{2B}AR mRNA being produced by these cells compared to other adenosine receptor transcripts. This valuable information contrasts with the gap in our knowledge regarding the role of the adenosine A_{2B}AR subtype on RV remodelling in PAH (for a review, see, e.g., [9, 16]). Herein, this study may contribute to elucidating this issue by evaluating the effect of A_{2B}AR in cell viability/proliferation and type I collagen production by CFs isolated from the RV myocardium of monocrotaline (MCT)-induced animal model of PAH, which is the most widely used experimental model for studying PAH in rats.

Materials and methods

PAH rat model

Male Wistar rats (*Rattus norvegicus*; Charles River, RGD Cat. No. 13508588, RRID:RGD_13508588) weighting 180–200 g were housed in groups of three to four animals inside ventilated Double Decker (38 cm high) cages with enriched environment and access to food and water *ad libitum*. The room temperature (21 °C) was kept constant and a regular light (07.30–19.30 h)–dark (19.30–07.30 h) cycle was imposed. The animals were acclimatized to these conditions for at least 10 days before their assignment to the two experimental groups: control (CTRL) and MCT-treated animals. MCT-induced PAH was generated by a single subcutaneous injection of MCT (60 mg/kg; MCT group; Crocotaline; Sigma-Aldrich, St. Louis, MO). Control rats were injected, at the same time, with an equal volume of sterile saline (CTRL group; NaCl 0.9%).

Twenty-one days after MCT or saline injection, the rats were euthanized by decapitation (Small Animal Decapitator, DCAP, World Precision Instruments) followed by exsanguination for heart tissues collection. Trained authorized personnel performed these procedures roughly between 9 and 10 a.m. in strict accordance with the recommendations of the European Convention for the Protection of Vertebrate Animals used for Experimental and Other Scientific Purposes (ETS 123), Directive 2010/63/EU, and Portuguese rules (DL 113/2013). The euthanasia method used in this study was privileged considering that (1) shared tissue usage is a common practice in our laboratory to reduce the number of experimental animals (“3R” principles), and that (2) functional neurochemistry assays are routinely performed in our laboratory using isolated nerve terminals from different parts of the rat brain, thus preventing usage of drugs (e.g., sedatives, general anesthetic drugs, and carbon dioxide), which might affect neuronal functions before sacrifice and compromise data interpretation.

RV histopathology assessment

The right heart hypertrophy was determined by Fulton’s index as the RV to the left ventricle plus septum (RV/(LV+S)) mass ratio. RV samples collected for histological analysis were stored in buffered 10% formaldehyde. After the initial fixation step, samples underwent dehydration (using ethanol in increasing concentrations), diaphanization (using xylene), and impregnation in liquid paraffin (54 °C). Paraffin-embedded RV samples were properly oriented inside metal frames before cutting into sections of 4- μ m thickness. Then, sections were stained with hematoxylin and eosin (H&E) or Picro-Sirius Red to evaluate cardiomyocyte cross-sectional area and interstitial fibrosis, respectively. For the cardiomyocyte cross-sectional area, transverse sections were digitally photographed (Olympus IX81, Tokyo, Japan) and blindly measured using the Cell F imaging software (Olympus, Tokyo, Japan). Fifty muscle fibers per animal (3–4 rats per group) were analyzed only considering nuclei-centered cells for the analysis of cardiomyocyte dimensions. Photomicrographs of longitudinal sections of the RV stained with Picro-Sirius Red were assessed using the ImageJ software® (version 1.8.0, U.S. National Institutes of Health, MD, USA) for automated analysis of collagen content, as previously described [17, 18]. Images were captured with a monochrome charge-coupled device camera using a 20 \times magnification objective. The extent of fibrosis was determined by calculating the percentage of the Picro-Sirius Red-stained area over the total microscopic field area using the same magnification for all samples. A minimum of four separate images obtained from different (non-overlapping) regions of the RV were captured per tissue section; four tissue sections were analyzed per animal. The results obtained per animal were averaged within the same group, CTRL and MCT, for subsequent statistical analysis.

Immunofluorescence confocal microscopy of RV slices

After dissecting the RV-free wall, ventricular strips were accurately isolated, stretched, pinned flat onto cork slices, and embedded in Shandon cryo-matrix (Thermo Scientific) before being frozen in a liquid nitrogen-isopentane mixture. Cryosectioned 10- μ m thickness slices of the RV were thawed and fixed in phosphate-buffered saline (PBS) containing 50% acetone and 2% paraformaldehyde (PFA). Following fixation, the slices were washed three times for 10 min each using PBS and incubated for 2 h with a blocking buffer containing 10% fetal bovine serum (FBS), 1% bovine serum albumin (BSA), and 0.3% Triton X-10 in PBS. After blocking and permeabilization, the sections were incubated overnight at 4 °C with anti-vimentin (1:150, mouse, DAKO, UK) and anti-A_{2B}AR (1:50, rabbit, #AAR-003, Alomone Labs) antibodies made-up in a PBS-based incubation buffer containing 5% FBS, 1% BSA, and 0.3% Triton X-100. Following washout of the primary antibody with PBS (3 cycles of 10 min), tissue samples were incubated with species-specific secondary antibodies (Alexa Fluor 568-labelled anti-mouse and Alexa Fluor 488-labelled anti-rabbit; Molecular Probes, Invitrogen, USA) in the dark for 2 h, at room temperature. Finally, the glass slides containing the RV sections were mounted using VectaShield medium with 4'-6-diamidino-2-phenylindole (DAPI) to counterstain the nuclei (H-1200; Vector Labs). Observations were performed and analyzed using a laser-scanning confocal microscope (Olympus Fluo View, FV1000, Tokyo, Japan). The relative amount of vimentin-positive fibroblasts per RV tissue slice was assessed using the ImageJ software® (version 1.8.0, U.S. National Institutes of Health, MD, USA) with a similar strategy to that used for collagen quantification [17, 18]. A minimum of two separate images, captured from different (non-overlapping) regions of the RV, were obtained per tissue section using a 20 \times magnification objective. Four tissue sections were analyzed per animal. Statistical analysis was performed using four animals per treatment group, CTRL and MCT.

Cardiac fibroblast cell cultures

Isolation of RV cardiac fibroblasts and cell culture conditions

Rat CFs were isolated from the RV of CTRL and MCT animal groups, 21 days after injecting MCT or saline (CTRL). The cells were obtained by the explant technique in which fibroblasts migrate from minced tissue and grow in a fibroblast growth medium [19]. The cells were cultured on 96-well plastic-bottom plates using DMEM medium supplemented with 15% FBS, 1% of amphotericin B, and 1% of penicillin/

streptomycin, at 37 °C in a humidified atmosphere of 95% air and 5% CO₂. The medium was replaced twice a week. Primary cultures were maintained until they reached near confluence (~3–4 weeks). Adherent cells were enzymatically detached using a 0.04% trypsin-EDTA solution containing 0.025% type I collagenase in PBS. The resulting cell suspensions were cultured and maintained under the same conditions as mentioned above. All the experiments were performed in the first subculture [13, 14, 20–22].

Cell viability/proliferation assay

Viability/proliferation studies were performed using the MTT assay as previously described [12–14]. Rat CFs were seeded in flat plastic-bottom 96-well plates at a density of 3×10^4 cells/mL and cultured in supplemented DMEM as described before. Cell cultures were routinely monitored by phase contrast microscopy and characterized on days 1, 7, 14, 21, and 28. The MTT assay consists of the reduction of 3-[4,5-dimethylthiazol-2-yl]-2,5-diphenyltetrazolium bromide (MTT) to a purple formazan reaction product by metabolically viable cells. During the last 4 h of each test period, the cells were incubated with 0.5 mg/mL of MTT in the conditions referred to above. Then, the medium was carefully removed and decanted, and the stained product dissolved with DMSO before absorbance (A) determination at 600 nm using a microplate reader spectrometer (Synergy HT Multi-Mode Microplate Reader, BioTek Instruments). The results were expressed as A/well.

Type I collagen determination

Type I collagen determination was performed using the Sirius Red staining assay. Rat CFs were cultured following the same protocol as described for the viability/proliferation studies [12–14]. The staining protocol was adapted from a previous study [23]. The cell layers were washed twice in PBS before cells fixation with Bouin's fluid for 1 h. The fixation fluid was removed by suction and the culture plates were washed by immersion in running tap water for 15 min. The culture dishes were then allowed to air-dry before adding the Picro-Sirius Red dye (Direct Red 80). The cells were stained with the dye for 1 h under mild shaking on a microplate shaker. To remove the non-bound dye, the stained cells were washed with 0.01 N HCl and then dissolved in 0.1 N NaOH for 30 min at room temperature using a microplate shaker. Optical density was measured at 550 nm using 0.1 N NaOH as blank [14, 23]. The results were expressed as A/well.

Immunofluorescence staining of cardiac fibroblasts

Rat CFs were seeded in chamber slides at a density of 2.5×10^4 cells/mL and allowed to grow for 7 days (see, e.g.,

[12–14]). Cultured cells were fixed in 4% PFA in PBS for 10 min, washed 3 times in PBS (10 min each), and, subsequently, incubated with blocking buffer I (10% FBS, 1% BSA, 0.1% Triton X, 0.05% NaN₃) for 1 h. Primary antibodies diluted in blocking buffer II (5% FBS, 1% BSA, 0.1% Triton X, 0.05% NaN₃) were applied [mouse anti-porcine vimentin 1:250 (DAKO); goat anti-human DDR2 1:25 (Santa Cruz); mouse anti-human α -smooth muscle actin (SMA)-FITC 1:250 (Sigma); rabbit anti-human A_{2B}AR (2nd extracellular loop, 36 kDa) 1:50 (#AAR-003, Alomone Labs)] and the slides incubated overnight at 4 °C. The cells were then washed 3 times in PBS 1 \times (10 min each). The donkey anti-mouse IgG Alexa Fluor 488 (1:1000), donkey anti-rabbit Alexa Fluor Donkey 488 (1:1000), and donkey anti-goat IgG Alexa Fluor 633 (1:1000) secondary antibodies (Invitrogen) were diluted in blocking buffer II and incubated in the dark for 2 h, at room temperature. A final wash step was performed with PBS and, then, the glass slides were mounted with VectaShield medium with DAPI (Vector Laboratories) and stored at 4 °C. Observations were performed and analyzed using a laser-scanning confocal microscope (FV1000, Olympus) [12, 14, 24, 25].

SDS-PAGE and Western blot analysis

CFs were harvested and homogenized in a lysis buffer composed of 50 mM Tris-HCl (pH 8.0), 150 mM NaCl, 0.5% sodium deoxycholate, 1% Triton-X-100, 0.1% SDS, and a protease inhibitor cocktail. Protein quantification was assessed using the BCA protein assay kit according to the manufacturer's instructions (Pierce, Rockford, IL, USA). Equal amounts of protein per sample (150 μ g/lane) were resolved by SDS-PAGE under reducing conditions (i.e., the samples were solubilized in SDS reducing buffer containing 0.125 mM Tris-HCl, 4% SDS, 0.004% bromophenol blue, 20% glycerol, and 10% 2-mercaptoethanol, pH 6.8 at 70 °C for 10 min) using 10% polyacrylamide gels, and electrotransferred onto PVDF membranes (Millipore, MA, USA). The membranes were blocked for 1 h in Tris-buffered saline (TBS: 10 mM Tris-HCl, pH 7.5, 150 mM NaCl) containing 0.05% Tween 20 + 5% BSA, and then probed overnight at 4 °C with rabbit anti-human A_{2B} (second extracellular loop, 37 kDa) 1:200 (#AAR-003, Alomone Labs, Jerusalem, Israel) in the above-mentioned blocking buffer. Then, the membranes were washed three times for 10 min in 0.1% Tween 20 in TBS before their incubation with donkey anti-rabbit IgG (HRP) 1:70,000 (Abcam Plc, Cambridge, UK) secondary antibody for 120 min at room temperature. For normalization purposes, the membranes were also incubated with a rabbit anti-human α -tubulin (50 kDa) 1:2500 (#ab6046, Abcam). For the antibody specificity test, the rabbit anti-A_{2B}AR primary antibody was pre-adsorbed with a 10-fold molar excess of its blocking peptide (#BLP-AR003, Alomone Labs, Jerusalem, Israel) corresponding to amino acid residues 147–166

of the human A_{2B} AR second extracellular loop. After washing the membranes 3 times for 10 min, the antigen-antibody complexes were visualized by chemiluminescence with the Clarity Western ECL Substrate Kit (Bio-Rad Laboratories, Hercules, CA, USA) using the ChemiDoc MP imaging system (Bio-Rad Laboratories, Hercules, CA, USA). Gel band image densities were quantified with the ImageJ software (National Institute of Health, Bethesda, MD, USA).

Reagents and materials

Amphotericin B solution, penicillin-streptomycin, Direct Red 80 (Picro-Sirius Red 80, $C_{45}H_{26}N_{10}O_{21}S_6Na_6$), trypsin-EDTA solution, FBS, PBS, 5'-*N*-ethylcarboxamidoadenosine (NECA), 2-(2-furanyl)-7-[3-(4-methoxyphenyl)propyl]-7H-pyrazolo[4,3-*e*][1,2,4]triazolo[1,5-*c*]pyrimidin-5-amine (SCH442416), and 4-[2-[[6-amino-9-(nethyl- β -D-ribofuranuronamidoyl)-9H-purin-2-yl]amino]ethyl] benzene propanoic acid hydrochloride (CGS21680) were from Sigma-Aldrich (St. Louis, MO, USA). 8-[4-[4-(4-Chlorophenyl)piperazine-1-sulfonyl]phenyl]-1-propyl xanthine (PSB603) was from Tocris Cookson Inc. (Bristol, UK). Cell culture plates: 96-well plastic-bottom plates were purchased from Corning (New York, USA); cell culture chamber slides for confocal microscopy: glass-bottom chamber slides were purchased from Nunc (New York, USA). CGS21680, NECA, PSB603, and SCH442416 were diluted in dimethyl sulfoxide (DMSO); all other drugs were prepared in distilled water. Regarding solutions storage (as frozen aliquots at -20 °C) and dilution, pH control, and DMSO (maximum 0.05% v/v) testing, we followed that described in previous publications from our group [21, 22].

NECA (1–30 μ M) and CGS21680 (3 and 10 nM) were used as enzymatically stable adenosine analogues to activate A_{2B} AR and A_{2A} AR in CFs, respectively. PSB603 and SCH442416 were used as potent and selective A_{2B} AR and A_{2A} AR antagonists, respectively. PSB603 displays <17,000-fold selectivity for A_{2B} AR over other adenosine receptors [26], and SCH442416 displays >23,000-fold selectivity for A_{2A} AR with minimal affinity for other adenosine receptors up to >10 μ M concentrations [27].

Presentation of data and statistical analysis

Data graphs and statistical analysis were carried out using the Graph Pad Prism 9.1.0 software (La Jolla, CA, USA). Data are expressed as mean \pm SEM, unless otherwise noted, from an *n* number of individuals. No predetermined sample size calculation was performed. The D'Agostino–Pearson (omnibus K^2) test was used to check for normality of data distribution; $p < 0.05$ values indicate that data passed the normality test. Student's unpaired *t*-test or one-way analysis of variance (ANOVA), either corrected or uncorrected for multiple comparisons using the Bonferroni's or the Fisher's

LSD tests, respectively, was applied only if *F* was significant and there was no variance inhomogeneity; few outliers were identified using the ROUT method with a $Q = 1\%$. $p < 0.05$ (two-tailed) values were considered statistically significant.

Results

MCT-induced PAH model

As the disease progresses, the animals treated with MCT grew less (gained less body weight) than their control littermates; the body weight of MCT-treated animals was 15% less ($p < 0.05$) than control rats at sacrifice day, i.e., 21 days after MCT administration (Fig. 1A). MCT-treated animals exhibited marked RV hypertrophy indicated by the increase of Fulton's index, i.e., the ratio between the mass of the RV over that of the LV plus the septum (RV/(LV+S)) (Fig. 1B). The histopathological analysis of tissue sections from MCT-treated rats revealed hypertrophy of RV cardiomyocytes ($p < 0.05$) compared to control littermates (Fig. 1C and 1E). These findings agree with data in the literature showing RV remodelling secondary to pulmonary pressure overload in animals with PAH [28]. However, at this disease stage, the RV of MCT-treated rats had no significant myocardial fibrosis as determined by the Picro-Sirius Red histochemical assay, which specifically identifies collagen deposition (Fig. 1D and 1F).

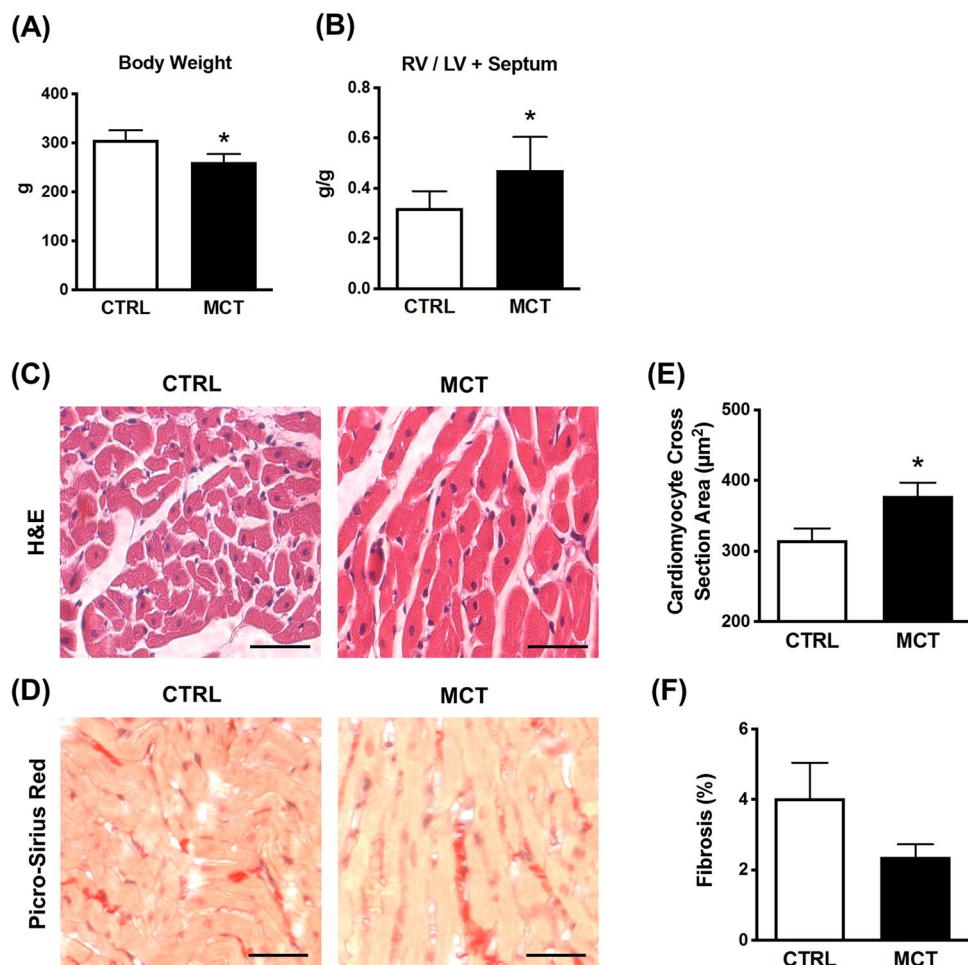
Immunophenotypic characterization of RV cardiac fibroblasts

CFs isolated from the RV of CTRL and MCT-treated adult rats displayed positive immunoreactivity against discoidin domain receptor 2 (DDR2) (Fig. 2B and 2E), a collagen-specific receptor tyrosine kinase, considered the most specific marker for CFs and myofibroblasts [29, 30]. The increase in DDR2 density suggests that CFs cultured from the RV of MCT-treated rats returned to an early activation status. Moreover, these cells also stain positively against vimentin (Fig. 2A), an intermediate protein filament considered a reliable fibroblast-cell marker [31], as well as against α -SMA (Fig. 2D), a myofilament protein that is typically expressed in activated fibroblasts (myofibroblasts) [32]. This staining pattern indicates that RV-originated CFs cultured under the present experimental conditions present an activated myofibroblast phenotype, which is the CFs lineage most commonly associated with myocardial remodelling [33].

Cardiac fibroblasts from MCT-treated rats proliferative more than cells from healthy controls

Data in Fig. 3A show that CFs isolated from the RV of MCT-treated rats are metabolically more active and/or proliferate

Fig. 1 Histomorphometric analysis of the RV of rats with pulmonary arterial hypertension (PAH) induced by monocrotaline (MCT). Shown in **A** is the body weight and in **B** is Fulton's index, which is the ratio between the mass of the RV over that of the LV plus the septum (RV/(LV+S)), of rats injected subcutaneously with saline (CTRL) or monocrotaline (MCT, 60 mg/kg) 21 days before the assessment. Tissue sections of the RV myocardium of both animal groups were stained with hematoxylin and eosin (H&E) (**C**) or Picro-Sirius Red (**D**). Scale bar: 50 μ m. In **E**, shown is the average cross-section area (μ m²) of at least 200 cardiomyocytes per animal group. In **F**, is represented the percentage of the Picro-Sirius Red positive staining (collagen deposition) to the total area of the micrograph, measured at least in 60 different tissue slices. Data are mean \pm SEM, $n = 5$ –9 animals/group. * $p < 0.05$ (Student's unpaired *t*-test) represents significant differences compared to the CTRL group



more (MTT assay) and produce higher amounts ($p < 0.05$) of type I collagen (Sirius Red assay) than the cells originated from their CTRL littermates. Interestingly, CFs from pressure-overloaded RV are more eager to reduce MTT (indicating increases in cell viability and/or proliferation; Fig. 3Ai) than to produce type I collagen (Fig. 3Aii) compared to the cells from healthy controls at this disease stage. In agreement with this theory, we observed a threefold ($p < 0.05$) increase in the density of vimentin-positive CFs in interstitial spaces of the RV obtained from MCT-treated rats compared to CTRL animals (Fig. 3B).

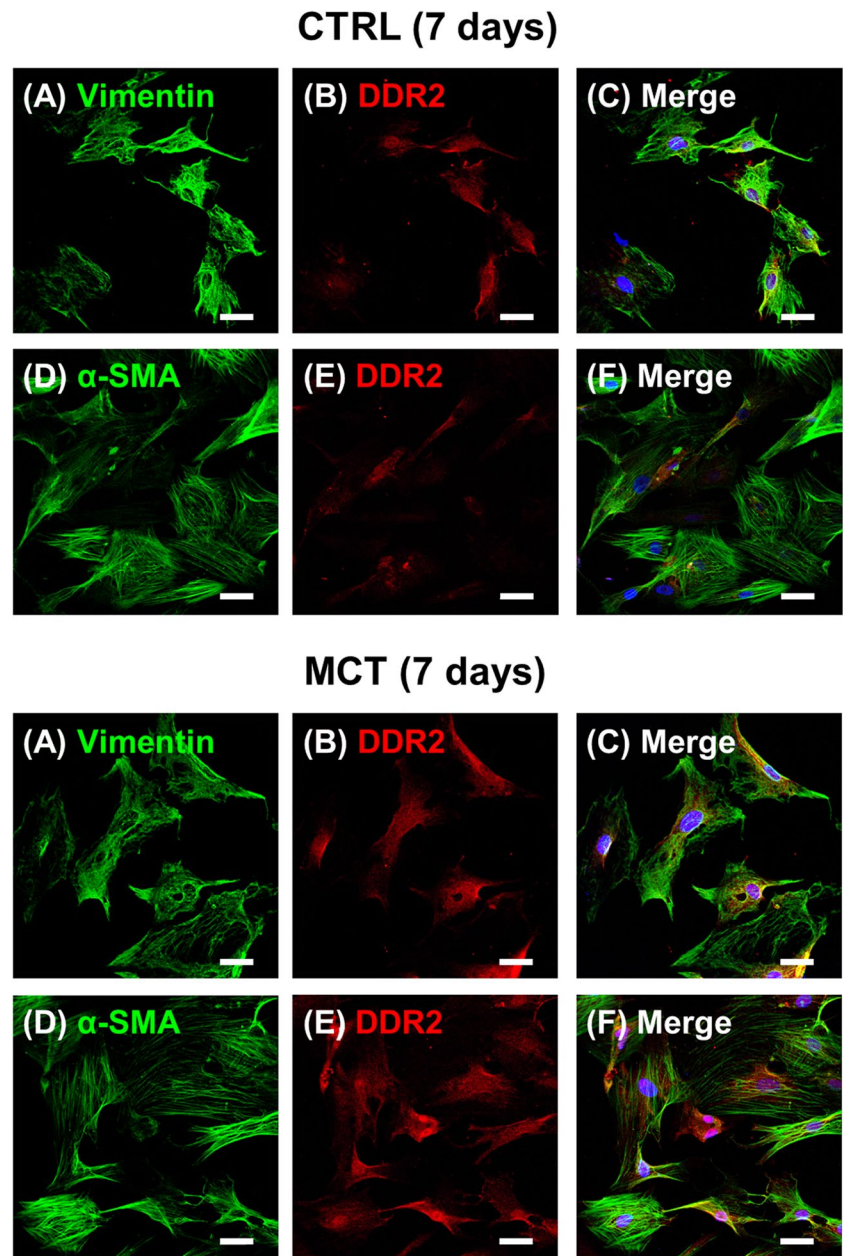
Cardiac fibroblasts from MCT-treated rats overexpress the A_{2B}AR

Using immunofluorescence confocal microscopy and Western blot analysis, we show here that CFs from MCT-treated rats overexpress the A_{2B}AR compared to CTRL littermates (Fig. 4). In the RV myocardium of MCT-treated rats, the A_{2B}AR immunoreactivity is more evident in interstitial spaces adjacent to hypertrophied cardiomyocytes, which display much weaker signalling against this receptor

(Fig. 4A). The A_{2B}AR-immunoreactive interstitial cell infiltrates comprise vimentin-positive CFs among other larger mononucleated cells (Fig. 4A), which are most probably mast and macrophage immunological cells similar to those overexpressing the A_{2B}AR in the fibrotic human lung [34]. Notably, the A_{2B}AR/vimentin double-immunolabelling significantly increases in the RV of PAH rats compared to their CTRL littermates (Fig. 4A). Likewise, we show here that CFs isolated from the RV of MCT-treated rats exhibit higher A_{2B}AR-immunoreactivity levels than cells from their control littermates, but also when this comparison was made with CFs obtained from the left ventricle (LV) of PAH rats (Fig. 4B).

The confocal microscopy findings are strengthened by immunoblot analysis data showing that the A_{2B}AR protein is upregulated in CFs isolated from the RV myocardium of MCT-treated rats compared to CTRL animals when these cells were allowed to grow for 28 days in culture (Fig. 4C). Interestingly, we detected two protein species: one close to the predicted molecular weight of the A_{2B}AR (~37 kDa) and a higher molecular mass (~45 kDa) isotype. The naturally occurring A_{2B}AR isotype is highly enriched in CFs isolated from the RV myocardium of MCT-treated rats compared

Fig. 2 Immunophenotypic characterization of cardiac fibroblasts (CFs) isolated from the RV of CTRL and MCT-treated rats on culture day 7. Confocal microscopy images show that CFs exhibit positive immunoreactivity against vimentin (a reliable fibroblast marker; green, **A**), α -smooth muscle actin (α -SMA, a myofilament protein typically expressed by activated myofibroblasts; green, **D**), and discoidin domain receptor 2 (DDR2, a collagen-specific receptor tyrosine kinase specifically expressed in CFs and myofibroblasts; red, **B** and **E**). Panels **C** and **F** show a merge of vimentin and DDR2, and α -SMA and DDR2, respectively. Nuclei are stained in blue with DAPI; yellow denotes colocalization. Scale bar: 30 μ m



to their CTRL littermates. Both bands completely disappear after pre-adsorption of the A_{2B} AR primary antibody with a 10-fold molar excess of the A_{2B} AR blocking peptide (#BLP-AR003, Alomone Inc., Jerusalem, Israel), which corresponds to amino acid residues 147–166 of the human A_{2B} AR second extracellular loop (negative control).

Activation of the A_{2B} AR promotes the growth of cardiac fibroblasts from the RV of MCT-treated rats

Figure 5 shows that the enzymatically stable adenosine analogue, NECA (1–30 μ M), concentration-dependently increased cell viability and/or growth (Fig. 5A) and type I collagen

(Fig. 5B) production by CFs obtained from the RV of both CTRL and MCT-treated rats. Yet, NECA-induced effects were much more evident ($p < 0.05$) in cultured cells isolated from rats with PAH. The pro-fibrotic effect of NECA (1–30 μ M) was more evident with the time of the cells in culture (days 21 and 28 > days 7 and 14). Under the present experimental conditions, NECA had an outstanding contribution to CFs viability/proliferation (MTT assay) (Fig. 5A) compared to type I collagen production (Sirius Red assay) by the same cells (Fig. 5B). Given that both 10 and 30 μ M NECA yield similar effects, the 10- μ M concentration was selected for subsequent experiments.

In contrast to NECA, the potent and selective A_{2A} AR agonist CGS21680 ($EC_{50} = 1.48$ –180 nM) had minimal

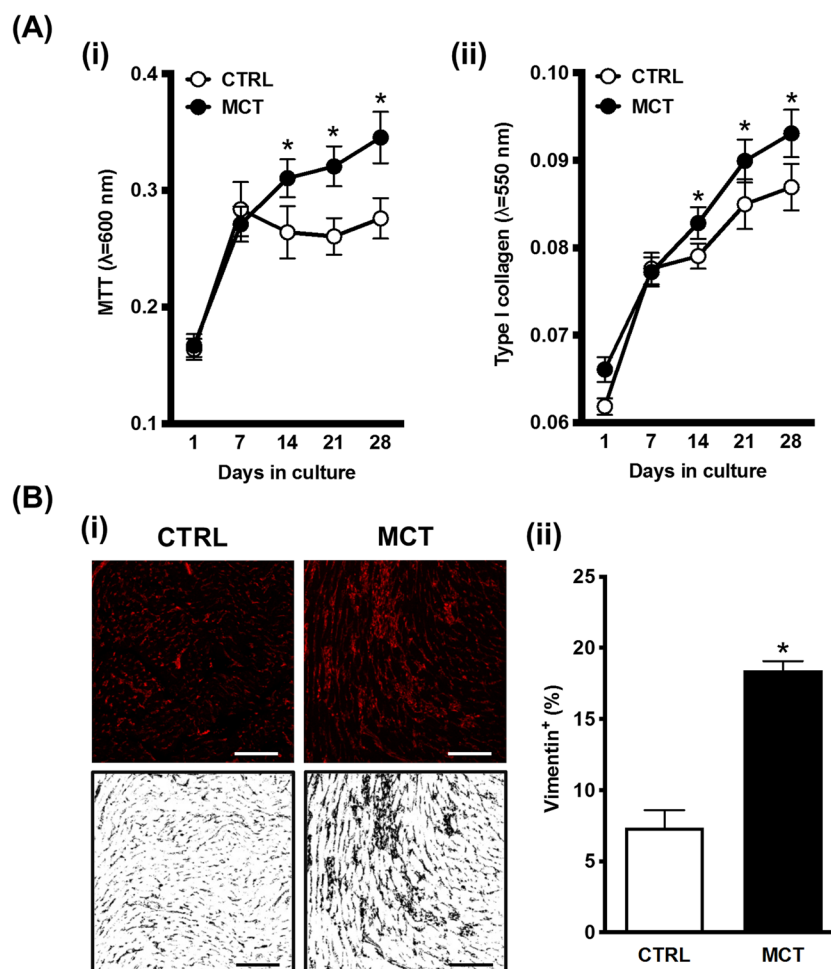


Fig. 3 Cardiac fibroblasts (CFs) isolated from the RV of MCT-treated rats exhibit increased cell viability/proliferation (MTT assay) and produce higher amounts of type I collagen (Sirius Red assay) than cells from healthy controls. Panel **A** illustrates changes in viability/proliferation measured by the MTT assay (**i**) and type I collagen production assessed by the Sirius Red staining (**ii**) in CFs isolated from CTRL ($n = 16$) and MCT-treated ($n = 18$) rats. The ordinates represent absorbance determinations at 600 nm and 550 nm per well at certain time points (1, 7, 14, 21, and 28 days), for the MTT assay (**Ai**) and the Sirius Red staining (**Aii**), respectively. Data are mean \pm SEM from an n number of individuals; the experiments were performed in trip-

licate. $*p < 0.05$ (ANOVA, one-way analysis of variance) compared to the CTRL group. In panel **B**, the red labelling in the upper panels represents vimentin-positive cells infiltrating RV interstitial spaces in CTRL and MCT-treated animals (**Bi**); scale bar: 100 μ m. The binary (black and white) representation of the images (bottom panels) was used for automatic quantification by the ImageJ software® (version 1.8.0, U.S. National Institutes of Health, Bethesda, MD, USA) (**Bii**). Data are mean \pm SEM; at least four individuals were analyzed per group. $*p < 0.05$ (Student's unpaired t -test) represents significant differences compared to the CTRL group

effects on CFs viability/proliferation (MTT assay) (Fig. 6A), as well as on type I collagen production (Sirius Red assay) (Fig. 6B). This was observed even when CGS21680 was used in the 3 to 10 nM concentration range that is known to be effective in other mesenchymal-originated cells, like subcutaneous fibroblasts and bone-marrow osteoblast progenitors [12, 22].

NECA exhibits the highest affinity for the A_{2B} AR subtype among all other adenosine analogues [35]. Considering that, despite this, it may also bind to other P1 adenosine receptors present in CFs, we set to investigate the involvement of the A_{2B} AR using the selective A_{2B} AR antagonist

PSB603 (100 nM), which displays >17,000-fold selectivity for A_{2B} AR over other adenosine receptors [26]. Co-application of PSB603 (100 nM) together with NECA (10 μ M) attenuated ($p < 0.05$) the effect of this adenosine receptor agonist on cell viability and/or proliferation of CFs isolated from the RV of MCT-treated rats (Fig. 7A), but no effects were observed in type I collagen production by the cells of these animals (Fig. 7B) nor of CTRL rats. The selective A_{2A} AR blocker, SCH442416 (10 nM) [27], did not modify the effects of NECA (10 μ M) on CFs viability/proliferation (Fig. 8A) and type I collagen production (Fig. 8B), under the same experimental conditions. Given these findings, one

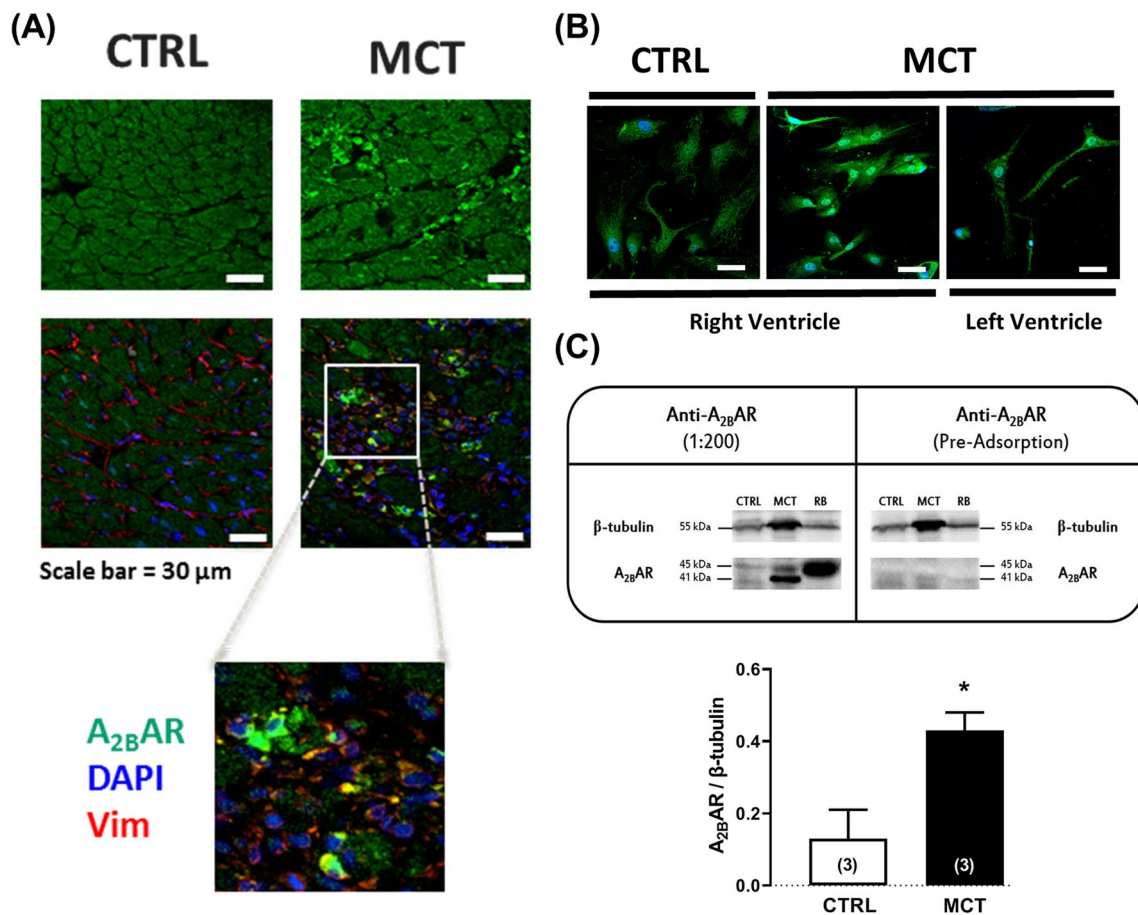


Fig. 4 Cardiac fibroblasts (CFs) isolated from MCT-treated rats over-express the adenosine A_{2B} receptor subtype. Shown are representative immunofluorescence confocal microscopy images of RV myocardium sections (**A**) and isolated CFs from the RV and LV myocardium (**B**) of CTRL and MCT-treated rats stained against A_{2B}AR (green) and vimentin (red). Nuclei are stained in blue with DAPI. Micrographs are representative of at least five different individuals and were obtained with a laser-scanning confocal microscope using the same acquisition settings. Scale bar: 30 μm. In **C**, shown are representative immunoblots to document the relative amounts of the A_{2B}AR in CFs isolated from the RV myocardium of CTRL and MCT-treated rats allowed to grow in culture for 28 days; gels were loaded with 150 μg protein amounts. Two protein species were recognized by the A_{2B}AR antibody (#AAR-003, Alomone Inc., Jerusalem, Israel) corresponding to a peptide near the predicted molecular weight of the A_{2B}AR

(~37 kDa) and a higher molecular mass (~45 kDa) isotype. Please note that the naturally occurring A_{2B}AR isotype is highly enriched in CFs isolated from the RV myocardium of MCT-treated rats compared to their CTRL littermates. Both bands fully disappeared after pre-adsorption of the A_{2B}AR primary antibody with a 10-fold molar excess of the A_{2B}AR blocking peptide (#BLP-AR003, Alomone Inc., Jerusalem, Israel) corresponding to amino acid residues 147–166 of the human A_{2B}AR second extracellular loop (negative control). The rat urinary bladder (RB) was used as a positive control for the A_{2B}AR. β-Tubulin (55 kDa) was used as a reference protein. Each bar represents pooled data from three different individuals; three replicas were performed in each experiment. The vertical bars represent SEM. **p* < 0.05 (Student's unpaired *t*-test) represents significant differences compared to the CTRL group

cannot exclude the synergistic participation of less dominant P1 receptor subtypes, namely A₁AR and A₃AR, in the A_{2B}AR-mediated promotion of type I collagen production by CFs of MCT-treated rats.

Discussion

We report here, for the first time, that activation of the adenosine A_{2B}AR subtype increases the metabolic activity and/or the proliferation and type I collagen production by cardiac

myofibroblasts isolated from the RV of healthy rats. More importantly, we provide evidence showing that these effects are bolstered in CFs overexpressing the A_{2B}AR obtained from animals presenting mild to moderate signs of PAH. Selective blockage of the A_{2B}AR activation with PSB603 attenuated NECA-induced increases in cell viability/proliferation of CFs isolated from MCT-induced PAH animals, without affecting the type I collagen production by the same cells.

PAH is a putatively fatal disorder characterized by increased pulmonary vascular resistance, which if left

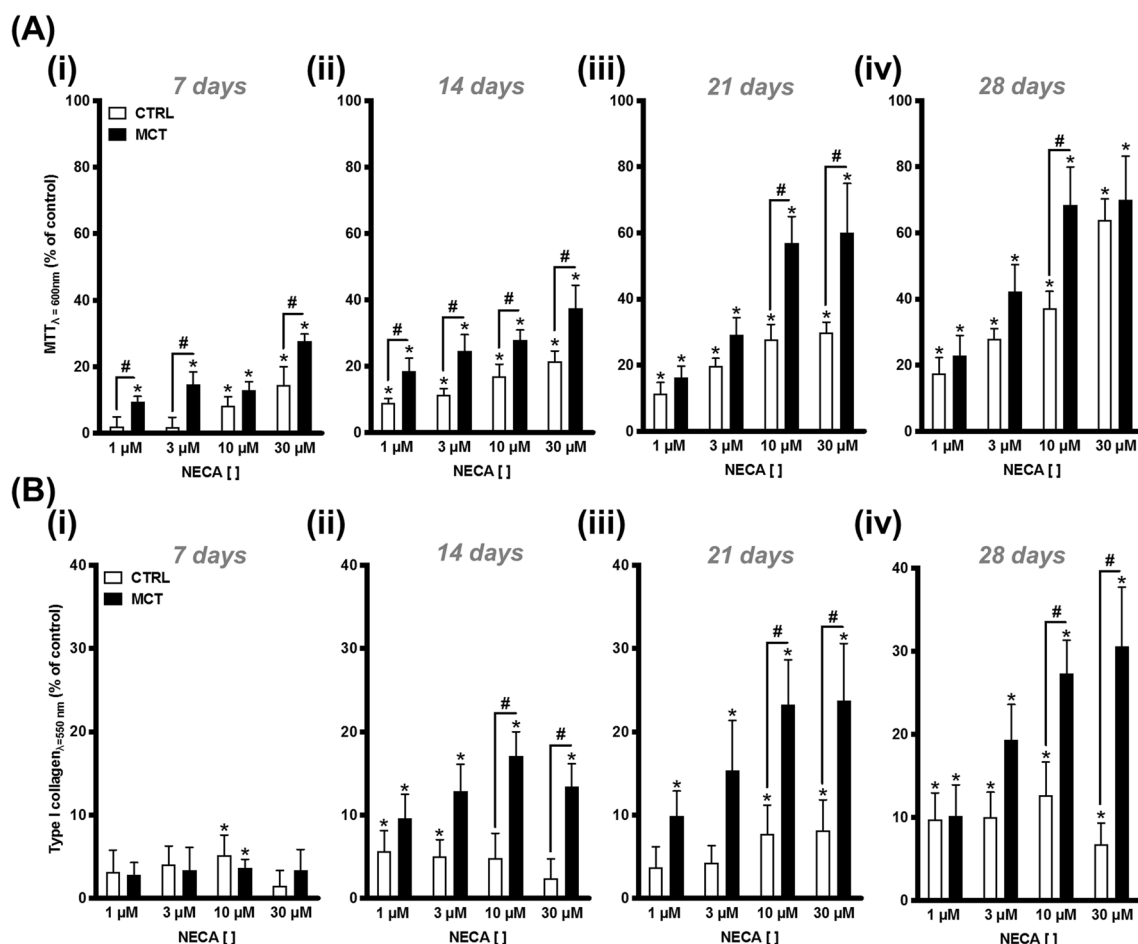


Fig. 5 The enzymatically stable adenosine analogue, NECA (1–30 μM), concentration-dependently increases cell viability/growth and type I collagen production by cardiac fibroblasts (CFs) from the RV of CTRL and MCT-treated rats. The ordinates represent NECA (1–30 μM)-induced changes in cell growth (MTT assay, **A**) and type I collagen production (Sirius Red assay, **B**) compared to the control situation using the same cell batch in the absence of the adenosine analogue at culture days 7 (**i**), 14 (**ii**), 21 (**iii**), and 28 (**iv**). Zero represents the similarity between the two values (NECA vs. control); positive

and negative values represent facilitation or inhibition of either cell growth or type I collagen production relative to control data obtained at the same time points. Each bar represents pooled data from three to six animals performed in triplicate. The vertical bars represent SEM. * $p < 0.05$ (ANOVA, one-way analysis of variance) represents significant differences from control values obtained in the absence of test drugs; # $p < 0.05$ (ANOVA, one-way analysis of variance) represents significant differences compared to the CTRL group

untreated rapidly progresses to right ventricular failure, irreversible dysrhythmias, and death [1]. Besides pulmonary vascular abnormalities, cardiac maladaptive remodelling (e.g., fibrosis), vasoconstriction, inflammation, and thrombosis are also common features of this progressive disorder. Currently approved drug treatments for PAH focus primarily on reducing pulmonary vascular resistance through the use of prostacyclin analogues, endothelin-1 receptor antagonists, phosphodiesterase-5 inhibitors, and soluble guanylate cyclase activators. Yet, these interventions have a limited impact on myocardial remodelling [3, 4]. This gap in our knowledge paves the way for novel therapeutic approaches to specifically target the pathological remodelling process evolving in the myocardium of PAH patients, as these

changes critically contribute to the fatal outcomes associated with this disease condition.

The natural course of RV remodelling secondary to PAH is characterized by an early compensatory phase comprising RV hypertrophy and improvement of systolic parameters, which help to preserve the cardiac output, with minimal fibrosis [1]. If the pressure overload is maintained, the RV enters into a decompensated phase resulting in a gradual decline of the RV systolic pressure and, consequently, of the cardiac output, which is accompanied by extensive myocardial fibrosis and dilation of cardiac chambers [36]. Several mechanisms may contribute to the shift from a compensated to a decompensated state, but myocardial fibrosis certainly represents one of the most relevant [37].

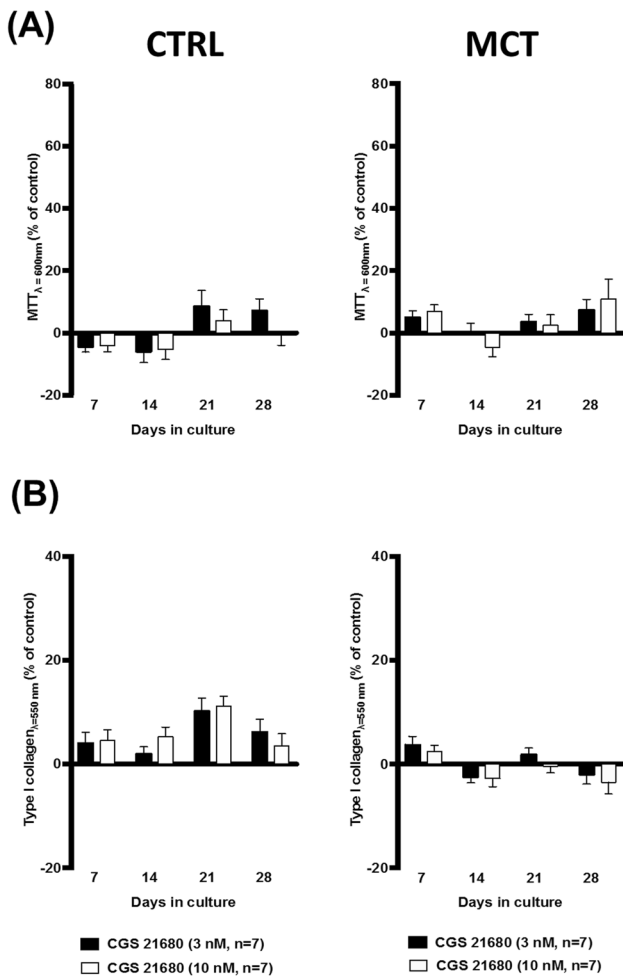


Fig. 6 Effects of the selective A_{2A} receptor agonist, CGS216980 (3–10 nM), on cell viability/growth and type I collagen production by cardiac fibroblasts (CFs) from the RV of CTRL and MCT-treated rats. The ordinates represent CGS216980 (3–10 nM)-induced changes in cell growth (MTT assay, **A**) and type I collagen production (Sirius Red assay, **B**) compared to the control situation using the same cell batch in the absence of the A_{2A} AR agonist at culture days 7, 14, 21, and 28. Zero represents the similarity between the two values (CGS216980 vs. control); positive and negative values represent facilitation or inhibition of either cell growth or type I collagen production relative to control data obtained at the same time points. Each bar represents pooled data from 7 animals; 3 to 4 replicas were performed for each experiment. The vertical bars represent SEM. * $p < 0.05$ (ANOVA, one-way analysis of variance) represents significant differences from control values obtained in the absence of test drugs

The MCT-induced PAH model was selected due to its simplicity and reproducibility, including the ability to induce neuroendocrine and inflammatory activation that is required for rapid progression to RV failure [38]. In the present study, PAH animals grew slowly (gained less body weight) compared to their CTRL littermates from the post-injection day 7 onwards (Fig. 1A), which is aligned with previous findings in the literature [39, 40]. The morphometric analysis revealed an increase in Fulton's index (Fig. 1B) suggesting

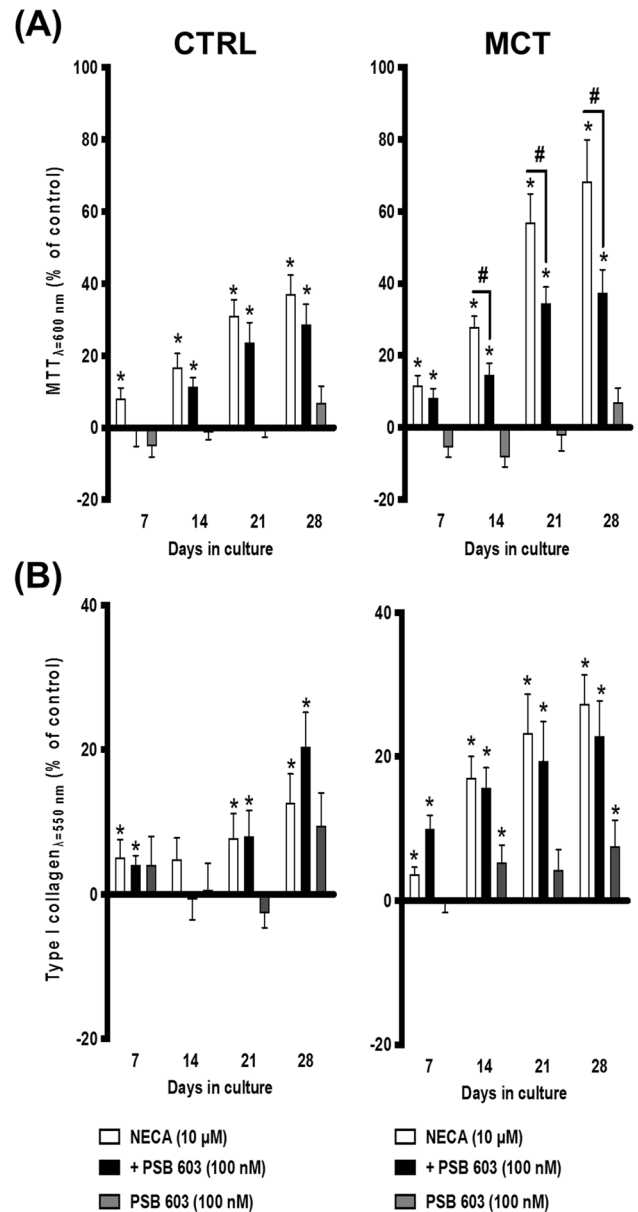


Fig. 7 Selective A_{2B} receptor blockage with PSB603 (100 nM) attenuates NECA-induced overgrowth of cardiac fibroblasts (CFs) from the RV of MCT-treated rats. NECA (10 μ M) with or without PSB603 (100 nM) was incorporated in culture media throughout the whole assay. The ordinates represent NECA- and/or PSB603-induced changes in cell growth (MTT assay, **A**) and type I collagen production (Sirius Red assay, **B**) compared to the control situation using the same cell batch in the absence of test drugs at culture days 7, 14, 21, and 28. Zero represents the similarity between the two values (drug vs. control); positive and negative values represent facilitation or inhibition of either cell growth or type I collagen production relative to control data obtained at the same time points. Each bar represents pooled data from 5 (CTRL) and 6 (MCT) animals; 3 to 4 replicas were performed for each experiment. The vertical bars represent SEM. * $p < 0.05$ (ANOVA, one-way analysis of variance) represents significant differences from control values obtained in the absence of test drugs; # $p < 0.05$ (ANOVA, one-way analysis of variance) represents significant differences compared to the effect of NECA alone

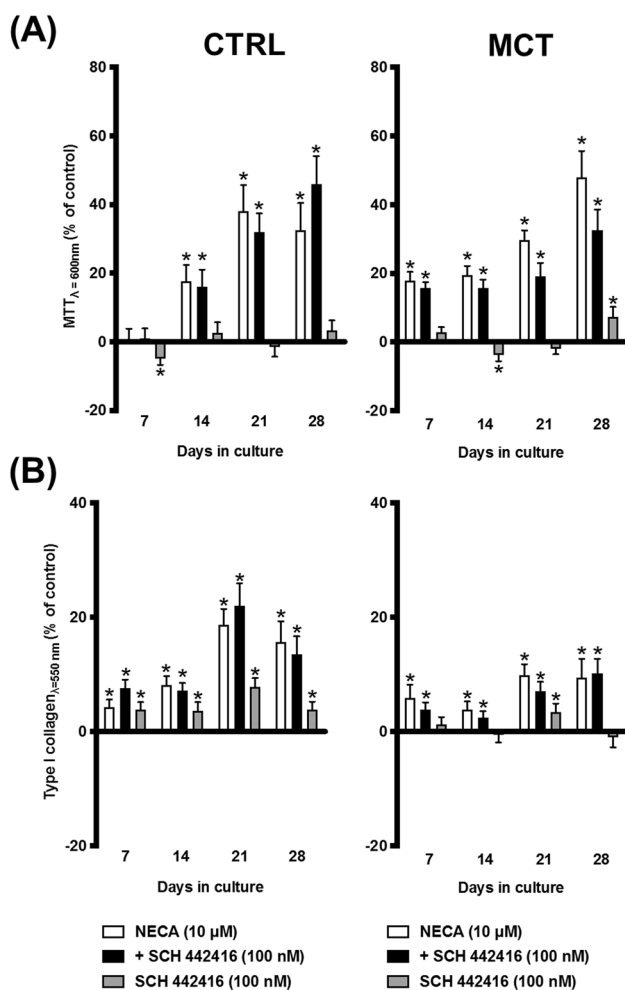


Fig. 8 Selective A_{2A} receptor blockage with SCH442416 (100 nM) did not modify NECA-induced overgrowth of cardiac fibroblasts (CFs) from the RV of MCT-treated rats. NECA (10 μ M) with or without SCH442416 (100 nM) was incorporated in culture media throughout the whole assay. The ordinates represent NECA- and/or SCH442416-induced changes in cell growth (MTT assay, **A**) and type I collagen production (Sirius Red assay, **B**) compared to the control situation using the same cell batch in the absence of test drugs at culture days 7, 14, 21, and 28. Zero represents the similarity between the two values (drug vs. control); positive and negative values represent facilitation or inhibition of either cell growth or type I collagen production relative to control data obtained at the same time points. Each bar represents pooled data from 8 animals; 3 to 4 replicas were performed for each experiment. The vertical bars represent SEM. $*p < 0.05$ (ANOVA, one-way analysis of variance) represents significant differences from control values obtained in the absence of test drugs

that MCT-treated rats exhibited RV hypertrophy [39, 40]. The histological assessment revealed that the cross-sectional area of RV cardiomyocytes was enlarged in MCT-treated rats compared to the CTRL group (Fig. 1C and 1E) [41, 42]. Overall, data demonstrate that a single injection of MCT caused mild to moderate pulmonary pressure overload leading to RV hypertrophy, which is a hallmark of PAH [7, 43].

Despite the aforementioned PAH features, the presence of RV myocardial fibrosis in the MCT-induced animal model has been a matter of debate in the literature. Failure to demonstrate interstitial or replacement fibrosis in MCT-treated rats assessed by the deposition of type I collagen has been claimed by some research groups [44–47]. In our hands, we observed a threefold increase in vimentin-positive CFs infiltrating the RV myocardium of MCT rats compared with healthy controls (Fig. 3B). The overgrowth of CFs in the RV myocardium of MCT-treated animals occurred in parallel with the hypertrophy of cardiomyocytes revealed as increases in the cross-section area of the cells vis-a-vis those obtained from healthy controls (Fig. 1C and 1E). Surprisingly, the Picro-Sirius Red assay detected minimal amounts of collagen in the myocardium 21 days after the MCT injection (Fig. 1D and 1F). This trend may be owed to the belated synthesis of type I collagen compared to the production of other ECM proteins (e.g., type III collagen) [48], in addition to early-to-intermediate stage features of myocardial remodelling comprising CFs overgrowth rather than collagen deposition (see above). It, thus, appears that in this animal model of PAH, the RV remodelling primarily involves cardiomyocyte hypertrophy, CFs overgrowth, and the myofibroblastic transformation of these cells towards the expression of α -SMA and DDR2 [49], rather than collagen deposition (fibrosis) in the myocardial interstitial spaces [7, 47, 50]. The incapacity to target CFs proliferation and these cells' differentiation into activated myofibroblasts may explain why currently available medications fail to effectively address the RV remodelling and, thus, the inexorable progression to RV failure associated with PAH [51].

CFs are the most abundant cell type in the heart [52], which along with cardiomyocytes play prominent roles in defining cardiac structure and function [53]. Given their abundance, strategic location within the cardiac interstitium, and ability to modulate their own and other cells' functions (e.g., cardiomyocytes, inflammatory cells, and endothelial cells), CFs play a sentinel role to detect myocardial injury states, as well as to transmit information to initiate reparative responses and to coordinate myocardial remodelling [54]. CFs proliferation and differentiation into myofibroblasts are critical features underlying cardiac fibrosis, which is one of the main pathological findings of heart failure. Cardiac fibrosis not only diminishes cardiac reserve but also increases the susceptibility to life-threatening dysrhythmias. Hence, from a clinical perspective, elucidating the mechanism(s) behind CFs proliferation and/or differentiation holds paramount importance to uncover novel pharmacological targets for PAH treatment.

Among the various autocrine/paracrine signalling messengers originating from pathologically stressed cells, adenine nucleotides and nucleosides emerge as important players in the regulation of CFs' growth and differentiation

[12–14]. Adenosine is a retaliatory metabolite playing important roles in myocardial reperfusion, hypertrophy, and remodelling. Extracellular adenosine levels rise dramatically in response to metabolic stress; the nucleoside can be released as such, via equilibrative nucleoside transporters, or can originate as a consequence of the extracellular ATP breakdown, via the ectonucleotidase cascade [55]. Adenosine exerts its biological effects by binding to P1 receptors (A_1 AR, A_{2A} AR, A_{2B} AR, and A_3 AR) [8]. Under pathological conditions, high extracellular levels of the nucleoside favor activation of low-affinity A_{2B} AR, which are normally silent under physiological conditions [21, 22, 56]. Emerging evidence indicates that pathological conditions favor A_{2B} AR-mediated “biased” signalling cascades depending on various factors, namely receptors cell trafficking and localization, post-translational modifications, and promiscuous coupling to other effector proteins (reviewed in [9]). Previous studies suggest a detrimental impact of the A_{2B} AR subtype in chronic lung diseases, particularly concerning lung and cardiac fibrosis [57, 58]. Despite all adenosine receptor subtypes are represented in rat CFs, the A_{2B} AR is the most abundant, followed by A_{2A} AR and A_1 AR subtypes, with minimal amounts detected for the A_3 AR [15, 59]. Regardless of their presence, the participation of adenosine receptors in the control of CFs growth, differentiation, and cardiac fibrosis is far from being completely understood (reviewed in [60]) and, so far, few studies investigated their role in the context of PAH [61–64].

CFs isolated from MCT-treated rats are metabolically more active and/or grow faster and overexpress A_{2B} AR compared to cells obtained from healthy controls. Upregulation of the A_{2B} AR was also observed in CFs from human patients with LV dysfunction secondary to valvulopathies [65]. Others have shown that CFs isolated from RV of MCT-induced PAH rats proliferate more than the cells from CTRL littermates [61]; these authors implicated in this mechanism calcium-dependent (SOCE/CaMKII) and calcium-independent (ERK1/2) pathways. Epigenetic reprogramming of mitochondrial metabolic pathways also seems to participate in CFs overgrowth observed in the RV of MCT-treated animals [62, 63]. In addition, the involvement of cyclic GMP-dependent pathways on collagen production by CFs isolated from the RV of mice subjected to pulmonary artery banding has been demonstrated, which further validates the use of medications, like sildenafil and riociguat, in the treatment of PAH [64].

The immunoblot analysis of cultured CFs extracts performed in our study detected two protein isoforms (see Fig. 4): one around 37 kDa (the predicted molecular weight of the A_{2B} AR) and another with a higher molecular mass (~45 kDa). The naturally occurring 37 kDa protein isoform is the main contributor to the A_{2B} AR enrichment in CFs isolated from the RV myocardium of MCT-treated rats. At this

point, one may only speculate that the higher molecular mass (~45 kDa) band existing both in CTRL and MCT-treated CFs might correspond to an A_{2B} AR protein species affected by post-translational modifications, most commonly due to glycosylation [66]. This assumption, as well as the pathophysiological meaning of these findings, certainly deserves to be fully elucidated in the future.

Our data show that the enzymatically stable adenosine analogue, NECA, increases the metabolic activity and/or the proliferation and type I collagen production by CFs obtained from both CTRL and MCT-treated rats, but these effects were much more evident in cells isolated from pressure-overloaded RV of rats with PAH. Here, NECA was used within a concentration range (1–30 μ M) known to activate the A_{2B} AR subtype (EC_{50} of 2 μ M) [67–69]. The involvement of the A_{2B} AR subtype was confirmed by blocking NECA-induced cell viability/proliferation with the selective A_{2B} AR antagonist, PSB603, whereas the A_{2A} AR antagonist, SCH442416, had no effect under the same experimental conditions. The potent and selective A_{2A} AR agonist, CGS21680 (EC_{50} = 1.48–180 nM), failed to modify growth and type I collagen production by CFs isolated from both control and MCT-treated rats, even when applied in concentrations (3 nM and 10 nM) high enough to increase the proliferation of other mesenchymal-originated cells [12, 22]. These findings suggest a dominant participation of the A_{2B} AR subtype in the pro-fibrotic effect of NECA, while minimizing the involvement of the A_{2A} AR subtype in this mechanism, regardless of data approaching pulmonary microvessel remodelling and hypertrophy suggesting that targeting the latter receptor may be beneficial for treating PAH and concomitant RV failure (reviewed in [16]). The lack of A_{2A} AR-mediated effects in moderate to severe disease stages is not surprising, since rats with PAH-induced RV failure exhibit reduced A_{2A} AR levels in the myocardial tissue [16]. Moreover, the pro-fibrotic effect of the A_{2B} AR subtype in the RV of PAH rats replicates that were verified in the lung [70] and kidney [71] preparations, thus strengthening its role in fibrotic processes.

Interestingly, selective blockage of A_{2B} AR activation with PSB603 attenuated NECA-induced increases in cell viability/proliferation of CFs from the RV of PAH rats with a minor (if at all) effect on type I collagen production by these cells. Parallel histopathological assays carried out in the same myocardial samples fully agree with data obtained in isolated CFs, given that the RV of MCT-treated rats displays extensive interstitial infiltration by triple-positive vimentin/DDR2/ α -SMA CFs adjacent to hypertrophied cardiomyocytes, but shown only small amounts of collagen in the same regions as demonstrated by the Picro-Sirius Red staining. Thus, one may speculate that endogenously generated adenosine, acting via A_{2B} AR, may contribute to CFs growth and myofibroblastic differentiation of these cells with only a minimal influence on ECM deposition at this disease stage.

Despite the low-affinity A_{2B} AR subtype has been extensively implicated in multiple pathological conditions [72], supporting its pivotal role in excessive CFs growth in the RV myocardium of PAH rats, one cannot discount the participation of other NECA-sensitive P1 receptors in collagen production. Considering that NECA-induced collagen production by cultured CFs of PAH rats transcended that obtained in CTRL animals, yet no prevention of the NECA effect was obtained upon blocking A_{2B} AR (with PSB603) and A_{2A} AR (with SCH442416), one may hypothesize the participation of minority A_1 AR and/or A_3 AR in this endeavor [15, 59]. Despite no specific involvement of A_1 AR and/or A_3 AR has been addressed in the context of PAH has not been addressed, evidence exists that the expression and signalling via A_1 AR and/or A_3 AR may increase fibrosis in several pathological conditions [65, 73–76].

The A_{2B} AR subtype has been previously implicated in experimental cardiac fibrosis induced in mice [77], rats [78], and humans [78, 79]. In CFs from healthy human subjects, NECA (10 μ M) increased the expression of α -SMA and α -1 procollagen, as well as the production of soluble collagen; these effects were effectively blocked by GS-6201 (100 nM), a selective A_{2B} AR antagonist [78, 79], which was also able to attenuate pulmonary fibrosis [70]. Similar to the antiproliferative activity of the A_{2B} AR antagonist, PSB603, on CFs from the RV of PAH rats, Zhang and co-workers showed that GS-6201 could reduce myocardial fibrosis in a rat model of myocardial infarction [78]. In another study, Karmouty-Quintana et al. showed that the A_{2B} AR activation promotes endothelin-1 and IL-6 release from endothelial cells and pulmonary artery myocytes, thus contributing to vessel wall remodelling and PAH progression [80]. Despite these findings, the A_{2B} AR-mediated pro-fibrotic activity in the heart is not consensual [67, 81–83]. Some authors claim that adenosine inhibits collagen synthesis [84] and mitogenesis [67] of CFs in adult rats, thus supporting the anti-fibrotic action of the nucleoside via A_{2B} AR activation in an “*in vivo*” animal model of myocardial infarction [83]. The A_{2B} AR was also involved in the inhibition of ET-1-induced cardiac fibrosis [85]. Likewise, overexpression of A_{2B} AR decreased collagen synthesis, while silencing the A_{2B} AR gene with a siRNA had the opposite effect [82]. Nevertheless, a controversy was installed in the same work as authors found that increasing concentrations of the enzymatic-stable adenosine analogue, NECA, favored, instead of preventing, collagen synthesis from A_{2B} AR overexpressing CFs [82], which fully agrees with our findings using primary CFs cultures from adult rats with PAH. The cardiac anti-fibrotic activity of the hybrid molecule, VCP746, is even more complicated to interpret, as this compound displays A_1 AR agonist properties while also binding bivalently with high affinity to A_{2B} AR [86].

Most studies reporting protective roles of the A_{2B} AR in PAH have focused on its involvement in vascular

remodelling, rather than on its role in subsequent RV myocardium overload and fibrosis; these studies often conclude on the A_{2B} AR enrolment by blocking this receptor activation with selective antagonists or gene silencing approaches (for a review, see, [9]). Under such conditions, elimination of the A_{2B} AR tonus is dependent on extracellular adenosine production/accumulation, which is a difficult issue to achieve given that the A_{2B} AR displays a low affinity for the nucleoside and, therefore, this receptor activation requires high extracellular adenosine concentrations. These controversies may reflect our incomplete understanding of the mechanism(s) driving cardiac remodelling in response to RV pressure overload in PAH. Variations in the experimental conditions (e.g., stage of the disease condition before culturing the cells; neonatal vs. adult cell cultures; the number of cell passages; stiffness of culture surfaces; and serum-starvation conditions) may additionally affect the phenotype, growth, differentiation, and function of cultured CFs. For instance, increasing the number of cell passages decreases CFs proliferation and leads to morphological changes associated with cell senescence [87]. Non-standardized drug application protocols may also introduce confounding effects; for instance, NECA inhibited proliferation and collagen synthesis when CFs were treated every 24 h for a maximum of 4 days [67]. In our study, we used rats with mild to moderate PAH before cell isolation and only the first-cell subcultures were assayed to avoid phenotypic de-differentiation artifacts. CF cultures were allowed to grow for 28 days in the presence of test drugs, which was directly compared with the control situation using the same cellular batch but without test drugs. Due to limited information regarding the role of A_{2B} AR on CFs proliferation and differentiation during the timeframe required for “*in vivo*” cardiac remodelling, we consider our results obtained in 28-day cultures derived from the RV myocardium of PAH animals a proxy of the real cells exposure to the nucleoside. Nevertheless, the current study has also potential limitations, since (i) we only assessed MCT-induced animals presenting mild to moderate PAH signs, and did not investigate (ii) how signalling events downstream A_{2B} AR activation could modulate cardiac fibrosis in PAH, nor (iii) did we explore the putative involvement of minority A_1 AR and/or A_3 AR in the pro-fibrotic effect of NECA.

In conclusion, this study provides the first evidence that adenosine, via A_{2B} AR activation, plays a pivotal role to increase cell viability/proliferation and myofibroblast differentiation of CFs from pressure-overloaded RV myocardium of rats with mild to moderate PAH. These findings highlight the putative therapeutic relevance of targeting CFs viability/growth and differentiation by blocking the A_{2B} AR activation to prevent cardiac remodelling and mitigate right heart failure in PAH patients. The clinical implications of our study extend beyond the RV myocardium, as targeting A_{2B} AR activation might also have a beneficial impact on

pulmonary vascular remodelling and lung fibrosis underlying this yet incurable disorder (see [9, 16]).

Acknowledgements The authors thank Mrs M. Helena Costa e Silva and Belmira Silva for their technical assistance, and Professor Fátima Gartner, Dr Alexandra Rema, and Dr Maria de Fátima Carvalho (Laboratory of Pathology, Department of Molecular Pathology and Immunology, ICBAS-UP) for helping with cardiac histology.

Availability of data and materials The data that support the findings of this study are available from the corresponding author upon reasonable request.

Authors' contribution Conceptualization, A.P.F.-S., P.C.-d.-S.; methodology, M.B.-G., B.B., E.M.-D., A.V., M.C., T.R., F.F., M.A.C.; formal analysis, M.B.-G., B.B., E.M.-D., A.V., M.C., T.R., F.F., M.A.C., A.P.F.-S., P.C.-d.-S.; investigation, M.B.-G., B.B., E.M.-D., A.V., M.C., T.R., F.F., M.A.C., A.P.F.-S., P.C.-d.-S.; resources, A.P.F.-S., P.C.-d.-S.; data curation, M.B.-G., B.B., E.M.-D., A.V., M.C., T.R., F.F., M.A.C.; writing—original draft preparation, M.B.-G., B.B., A.P.F.-S., P.C.-d.-S.; writing—review and editing, M.B.-G., B.B., A.P.F.-S., P.C.-d.-S.; supervision, F.F., M.A.C., A.P.F.-S., P.C.-d.-S.; project administration, P.C.-d.-S.; funding acquisition, A.P.F.-S., P.C.-d.-S. All authors have read and agreed to this version of the manuscript.

Funding Open access funding provided by FCTIFCCN (b-on). This research was partially supported by Fundação para a Ciência e a Tecnologia (FCT, FEDER funding, projects PTDC/DTP-FTO/0802/2012, PEst-OE/SAU/UI0215/2014, UID/BIM/4308/2016, UID/BIM/4308/2019, UIDB/04308/2020, and UIDP/04308/2020). P.C.S. also received financial support from FCT and Aga Khan Development Network (project #541708048). The funders had no role in study design, data collection and analysis, the decision to publish, or the preparation of the manuscript. M.C. and B.B. received a PhD scholarship from FCT (SFRH/BD/81414/2011 and SFRH/BD/104114/2014, respectively).

Compliance with ethical standards

Conflicts of interest The authors declare no competing interests.

Ethical approval Animal handling and experiments were performed following the Guide for the Care and Use of Laboratory Animals, published by the US National Institutes of Health (NIH Publication No. 85-23, Revised 2011), and followed the European Communities Council Directive (86/609/EEC). All procedures involving animals were approved by the competent national authority Direção Geral de Alimentação e Veterinária, and by the Animal Welfare Committee of ICBAS (No. 224/2017). All efforts were made to minimize animal suffering and to reduce the number of animals used according to the ARRIVE guidelines. This exploratory study was not pre-registered.

Open Access This article is licensed under a Creative Commons Attribution 4.0 International License, which permits use, sharing, adaptation, distribution and reproduction in any medium or format, as long as you give appropriate credit to the original author(s) and the source, provide a link to the Creative Commons licence, and indicate if changes were made. The images or other third party material in this article are included in the article's Creative Commons licence, unless indicated otherwise in a credit line to the material. If material is not included in the article's Creative Commons licence and your intended use is not permitted by statutory regulation or exceeds the permitted use, you will need to obtain permission directly from the copyright holder. To view a copy of this licence, visit <http://creativecommons.org/licenses/by/4.0/>.

References

- Vonk Noordegraaf A et al (2019) Pathophysiology of the right ventricle and of the pulmonary circulation in pulmonary hypertension: an update. *Eur Respir J* 53(1)
- Beckmann T et al (2022) Strategizing drug therapies in pulmonary hypertension for improved outcomes. *Pharmaceuticals (Basel)* 15(10)
- Dhoble S et al (2022) Comprehensive review on novel targets and emerging therapeutic modalities for pulmonary arterial hypertension. *Int J Pharm* 621:121792
- Sommer N et al (2021) Current and future treatments of pulmonary arterial hypertension. *Br J Pharmacol* 178(1):6–30
- Liu Y et al (2021) Inhibiting miR-1 attenuates pulmonary arterial hypertension in rats. *Mol Med Rep* 23(4)
- Tang Y et al (2022) MicroRNA-325-3p targets human epididymis protein 4 to relieve right ventricular fibrosis in rats with pulmonary arterial hypertension. *Cardiovasc Ther* 2022:4382999
- Sharifi Kia D, Kim K, Simon MA (2021) Current understanding of the right ventricle structure and function in pulmonary arterial hypertension. *Front Physiol* 12:641310
- Izerman AP et al (2022) International Union of Basic and Clinical Pharmacology. CXII: adenosine receptors: a further update. *Pharmacol Rev* 74(2):340–372
- Bessa-Goncalves M et al (2018) Is the adenosine A(2B) 'biased' receptor a valuable target for the treatment of pulmonary arterial hypertension? *Drug Discov Today* 23(6):1285–1292
- Vecchio EA, White PJ, May LT (2019) The adenosine A(2B) G protein-coupled receptor: recent advances and therapeutic implications. *Pharmacol Ther* 198:20–33
- Colin EE et al (2021) Endothelial cells in the pathogenesis of pulmonary arterial hypertension. *Eur Respir J* 58(3):2003957
- Costa MA et al (2011) On the role of subtype selective adenosine receptor agonists during proliferation and osteogenic differentiation of human primary bone marrow stromal cells. *J Cell Physiol* 226(5):1353–1366
- Pinheiro AR et al (2013) Histamine induces ATP release from human subcutaneous fibroblasts, via pannexin-1 hemichannels, leading to Ca²⁺ mobilization and cell proliferation. *J Biol Chem* 288(38):27571–27583
- Certal M et al (2015) Calcium signaling and the novel anti-proliferative effect of the UTP-sensitive P2Y₁₁ receptor in rat cardiac myofibroblasts. *Cell Calcium* 58(5):518–533
- Epperson SA et al (2009) Adenosine receptors and second messenger signaling pathways in rat cardiac fibroblasts. *Am J Physiol Cell Physiol* 296(5):C1171–C1177
- Alencar AKN et al (2017) Adenosine receptors as drug targets for treatment of pulmonary arterial hypertension. *Front Pharmacol* 8:858
- Hadi AM et al (2011) Rapid quantification of myocardial fibrosis: a new macro-based automated analysis. *Cell Oncol (Dordr)* 34(4):343–354
- Marcos R, Braganca B, Fontes-Sousa AP (2015) Image analysis or stereology: which to choose for quantifying fibrosis? *J Histochem Cytochem* 63(9):734–736
- Song K et al (2012) Heart repair by reprogramming non-myocytes with cardiac transcription factors. *Nature* 485(7400):599–604
- Certal M et al (2016) ADP-induced Ca²⁺ signaling and proliferation of rat ventricular myofibroblasts depend on phospholipase C-linked TRP channels activation within lipid rafts. *J Cell Physiol* 232(6):1511–1526
- Herman-de-Sousa C et al (2020) Opposing effects of adenosine and inosine in human subcutaneous fibroblasts may be regulated by third party ADA cell proteases. *Cells* 9(3):651

22. Herman-de-Sousa C et al (2022) A(2A) receptor-induced over-expression of pannexin-1 channels indirectly mediates adenosine fibrogenic actions by favouring ATP release from human subcutaneous fibroblasts. *Life Sci* 310:121080
23. Tullberg-Reinert H, Jundt G (1999) In situ measurement of collagen synthesis by human bone cells with a sirius red-based colorimetric microassay: effects of transforming growth factor beta2 and ascorbic acid 2-phosphate. *Histochem Cell Biol* 112(4):271–276
24. Alqallaf SM, Evans BA, Kidd EJ (2009) Atypical P2X receptor pharmacology in two human osteoblast-like cell lines. *Br J Pharmacol* 156(7):1124–1135
25. Noronha-Matos JB et al (2012) Role of ecto-NTPDases on UDP-sensitive P2Y(6) receptor activation during osteogenic differentiation of primary bone marrow stromal cells from postmenopausal women. *J Cell Physiol* 227(6):2694–2709
26. Borrmann T et al (2009) 1-alkyl-8-(piperazine-1-sulfonyl)phenylxanthines: development and characterization of adenosine A2B receptor antagonists and a new radioligand with subnanomolar affinity and subtype specificity. *J Med Chem* 52(13):3994–4006
27. Zheng J et al (2007) Protective roles of adenosine A1, A2A, and A3 receptors in skeletal muscle ischemia and reperfusion injury. *Am J Physiol Heart Circ Physiol* 293(6):H3685–H3691
28. Bradley SP et al (1996) Right ventricular pathology in chronic pulmonary hypertension. *Am J Cardiol* 78(5):584–587
29. Goldsmith EC et al (2010) The collagen receptor DDR2 is expressed during early cardiac development. *Anat Rec (Hoboken)* 293(5):762–769
30. Morales MO, Price RL, Goldsmith EC (2005) Expression of discoidin domain receptor 2 (DDR2) in the developing heart. *Microsc Microanal* 11(3):260–267
31. Agocha AE, Eghbali-Webb M (1997) A simple method for preparation of cultured cardiac fibroblasts from adult human ventricular tissue. *Mol Cell Biochem* 172(1–2):195–198
32. Brown RD et al (2005) The cardiac fibroblast: therapeutic target in myocardial remodeling and failure. *Annu Rev Pharmacol Toxicol* 45:657–687
33. Rohr S (2011) Cardiac fibroblasts in cell culture systems: myofibroblasts all along? *J Cardiovasc Pharmacol* 57(4):389–399
34. Varani K et al (2006) Alteration of adenosine receptors in patients with chronic obstructive pulmonary disease. *Am J Respir Crit Care Med* 173(4):398–406
35. Hinz S et al (2014) BAY60-6583 acts as a partial agonist at adenosine A2B receptors. *J Pharmacol Exp Ther* 349(3):427–436
36. Thandavarayan RA, Chitturi KR, Guha A (2020) Pathophysiology of acute and chronic right heart failure. *Cardiol Clin* 38(2):149–160
37. Sabbah BN et al (2023) Heart failure in systemic right ventricle: mechanisms and therapeutic options. *Frontiers in Cardiovascular Medicine*:9
38. Hill NS, Gillespie MN, McMurtry IF (2017) Fifty years of monocrotaline-induced pulmonary hypertension: what has it meant to the field? *Chest* 152(6):1106–1108
39. Jasenovc T et al (2022) Monocrotaline-induced pulmonary arterial hypertension and bosentan treatment in rats: focus on plasma and erythrocyte parameters. *Pharmaceuticals* 15. <https://doi.org/10.3390/ph15101227>
40. Qin T et al (2022) Protective effects of Dapagliflozin on the vulnerability of ventricular arrhythmia in rats with pulmonary artery hypertension induced by monocrotaline. *Bioengineered* 13(2):2697–2709
41. Yu M et al (2022) Paeoniflorin attenuates monocrotaline-induced pulmonary arterial hypertension in rats by suppressing TAK1-MAPK/NF- κ B pathways. *Int J Med Sci* 19(4):681–694
42. Dai Y et al (2019) Immunotherapy of endothelin-1 receptor type A for pulmonary arterial hypertension. *J Am Coll Cardiol* 73(20):2567–2580
43. Holda MK et al (2020) Changes in heart morphometric parameters over the course of a monocrotaline-induced pulmonary arterial hypertension rat model. *J Transl Med* 18(1):262
44. Hessel MH et al (2006) Characterization of right ventricular function after monocrotaline-induced pulmonary hypertension in the intact rat. *Am J Physiol Heart Circ Physiol* 291(5):H2424–H2430
45. van de Veerdonk MC, Bogaard HJ, Voelkel NF (2016) The right ventricle and pulmonary hypertension. *Heart Fail Rev* 21:259–271
46. Kwan ED et al (2021) Distinct time courses and mechanics of right ventricular hypertrophy and diastolic stiffening in a male rat model of pulmonary arterial hypertension. *Am J Physiol Heart Circ Physiol* 321(4):H702–H715
47. Holda MK et al (2020) Myocardial proteomic profile in pulmonary arterial hypertension. *Sci Rep* 10(1):14351
48. van den Borne SW et al (2010) Myocardial remodeling after infarction: the role of myofibroblasts. *Nat Rev Cardiol* 7(1):30–37
49. Kawano H et al (2000) Angiotensin II has multiple profibrotic effects in human cardiac fibroblasts. *Circulation* 101(10):1130–1137
50. Petrov VV, Fagard RH, Lijnen PJ (2002) Stimulation of collagen production by transforming growth factor-beta1 during differentiation of cardiac fibroblasts to myofibroblasts. *Hypertension* 39(2):258–263
51. Inampudi C et al (2020) Treatment of right ventricular dysfunction and heart failure in pulmonary arterial hypertension. *Cardiovasc Diagn Ther* 10(5):1659–1674
52. Hall C et al (2021) Complex relationship between cardiac fibroblasts and cardiomyocytes in health and disease. *J Am Heart Assoc* 10(5):e019338
53. Venugopal H et al (2022) Properties and functions of fibroblasts and myofibroblasts in myocardial infarction. *Cells* 11:1386. <https://doi.org/10.3390/cells11091386>
54. Diaz-Araya G et al (2015) Cardiac fibroblasts as sentinel cells in cardiac tissue: receptors, signaling pathways and cellular functions. *Pharmacol Res* 101:30–40
55. Guieu R et al (2020) Adenosine and the cardiovascular system: the good and the bad. *J Clin Med* 9:1366. <https://doi.org/10.3390/jcm9051366>
56. Beukers MW et al (2000) Why are A(2B) receptors low-affinity adenosine receptors? Mutation of Asn273 to Tyr increases affinity of human A(2B) receptor for 2-(1-Hexynyl)adenosine. *Mol Pharmacol* 58(6):1349–1356
57. Karmouty-Quintana H et al (2013) Adenosine A2B receptor and hyaluronan modulate pulmonary hypertension associated with chronic obstructive pulmonary disease. *Am J Respir Cell Mol Biol* 49(6):1038–1047
58. Karmouty-Quintana H, Xia Y, Blackburn MR (2013) Adenosine signaling during acute and chronic disease states. *J Mol Med (Berl)* 91(2):173–181
59. Headrick JP et al (2013) Cardiovascular adenosine receptors: expression, actions and interactions. *Pharmacol Ther* 140(1):92–111
60. Procopio MC et al (2021) Role of adenosine and purinergic receptors in myocardial infarction: focus on different signal transduction pathways. *Biomedicines* 9(2):204
61. Imoto K, Okada M, Yamawaki H (2018) Characterization of fibroblasts from hypertrophied right ventricle of pulmonary hypertensive rats. *Pflugers Arch* 470(9):1405–1417
62. Tian L et al (2018) Increased Drp1-mediated mitochondrial fission promotes proliferation and collagen production by right ventricular fibroblasts in experimental pulmonary arterial hypertension. *Front Physiol* 9:828
63. Tian L et al (2020) Epigenetic metabolic reprogramming of right ventricular fibroblasts in pulmonary arterial hypertension: a pyruvate dehydrogenase kinase-dependent shift in mitochondrial

- metabolism promotes right ventricular fibrosis. *Circ Res* 126(12):1723–1745
64. Rai N et al (2018) Effect of riociguat and sildenafil on right heart remodeling and function in pressure overload induced model of pulmonary arterial banding. *Biomed Res Int* 2018:3293584
 65. Del Ry S et al (2017) Adenosine receptors expression in cardiac fibroblasts of patients with left ventricular dysfunction due to valvular disease. *J Recept Signal Transduct Res* 37(3):283–289
 66. Linden J et al (1999) Characterization of human A(2B) adenosine receptors: radioligand binding, western blotting, and coupling to G(q) in human embryonic kidney 293 cells and HMC-1 mast cells. *Mol Pharmacol* 56(4):705–713
 67. Dubey RK et al (2001) A(2b) receptors mediate the antimitogenic effects of adenosine in cardiac fibroblasts. *Hypertension* 37(2):716–721
 68. Du X et al (2015) Adenosine A2B receptor stimulates angiogenesis by inducing VEGF and eNOS in human microvascular endothelial cells. *Exp Biol Med* (Maywood) 240(11):1472–1479
 69. Alnouri MW et al (2015) Selectivity is species-dependent: characterization of standard agonists and antagonists at human, rat, and mouse adenosine receptors. *Purinergic Signal* 11(3):389–407
 70. Sun CX et al (2006) Role of A2B adenosine receptor signaling in adenosine-dependent pulmonary inflammation and injury. *J Clin Invest* 116(8):2173–2182
 71. Tang J et al (2015) Effects of A2BR on the biological behavior of mouse renal fibroblasts during hypoxia. *Mol Med Rep* 11(6):4397–4402
 72. Eisenstein A, Patterson S, Ravid K (2015) The many faces of the A2b adenosine receptor in cardiovascular and metabolic diseases. *J Cell Physiol* 230(12):2891–2897
 73. Kalk P et al (2007) The adenosine A1 receptor antagonist SLV320 reduces myocardial fibrosis in rats with 5/6 nephrectomy without affecting blood pressure. *Br J Pharmacol* 151(7):1025–1032
 74. Shaikh G, Cronstein B (2016) Signaling pathways involving adenosine A2A and A2B receptors in wound healing and fibrosis. *Purinergic Signal* 12(2):191–197
 75. Yuan K et al (2008) Stimulation of ANP secretion by 2-Cl-IB-MECA through A(3) receptor and CaMKII. *Peptides* 29(12):2216–2224
 76. Yuan K et al (2005) Adenosine-stimulated atrial natriuretic peptide release through A1 receptor subtype. *Hypertension* 46(6):1381–1387
 77. Toldo S et al (2012) GS-6201, a selective blocker of the A2B adenosine receptor, attenuates cardiac remodeling after acute myocardial infarction in the mouse. *J Pharmacol Exp Ther* 343(3):587–595
 78. Zhang H et al (2014) Blockade of A2B adenosine receptor reduces left ventricular dysfunction and ventricular arrhythmias 1 week after myocardial infarction in the rat model. *Heart Rhythm* 11(1):101–109
 79. Zhong H, Belardinelli L, Zeng D (2011) Pro-fibrotic role of the A2B adenosine receptor in human cardiac fibroblasts. *J Card Fail* 17(8):S65
 80. Karmouty-Quintana H et al (2012) The A2B adenosine receptor modulates pulmonary hypertension associated with interstitial lung disease. *FASEB J* 26(6):2546–2557
 81. Lu D, Insel PA (2013) Hydrolysis of extracellular ATP by ectonucleoside triphosphate diphosphohydrolase (ENTPD) establishes the set point for fibrotic activity of cardiac fibroblasts. *J Biol Chem* 288(26):19040–19049
 82. Chen Y et al (2004) Functional effects of enhancing or silencing adenosine A2b receptors in cardiac fibroblasts. *Am J Physiol Heart Circ Physiol* 287(6):H2478–H2486
 83. Wakeno M et al (2006) Long-term stimulation of adenosine A2b receptors begun after myocardial infarction prevents cardiac remodeling in rats. *Circulation* 114(18):1923–1932
 84. Dubey RK, Gillespie DG, Jackson EK (1998) Adenosine inhibits collagen and protein synthesis in cardiac fibroblasts: role of A2B receptors. *Hypertension* 31(4):943–948
 85. Phosri S et al (2017) Stimulation of adenosine A(2B) receptor inhibits endothelin-1-induced cardiac fibroblast proliferation and alpha-smooth muscle actin synthesis through the cAMP/Epac/PI3K/Akt-signaling pathway. *Front Pharmacol* 8:428
 86. Vecchio EA et al (2016) The hybrid molecule, VCP746, is a potent adenosine A2B receptor agonist that stimulates anti-fibrotic signalling. *Biochem Pharmacol* 117:46–56
 87. Zhou Y, Richards AM, Wang P (2017) Characterization and standardization of cultured cardiac fibroblasts for ex vivo models of heart fibrosis and heart ischemia. *Tissue Eng Part C Methods* 23(7):422–433

Publisher's note Springer Nature remains neutral with regard to jurisdictional claims in published maps and institutional affiliations.